© 2019. Published by The Company of Biologists Ltd | Development (2019) 146, dev177659. doi:10.1242/dev.177659

RESEARCH ARTICLE

Sall4 regulates neuromesodermal progenitors and their descendants during body elongation in mouse embryos

Naoyuki Tahara[1,2,3], Hiroko Kawakami[1,2,3], Katherine Q. Chen[1], Aaron Anderson[1,*], Malina Yamashita Peterson[1], Wuming Gong[4], Pruthvi Shah[4], Shinichi Hayashi[1,2,3], Ryuichi Nishinakamura[5], Yasushi Nakagawa[2,3,6], Daniel J. Garry[2,3,4,7] and Yasuhiko Kawakami[1,2,3,‡]

ABSTRACT

Bi-potential neuromesodermal progenitors (NMPs) produce both neural and paraxial mesodermal progenitors in the trunk and tail during vertebrate body elongation. We show that *Sall4*, a pluripotency-related transcription factor gene, has multiple roles in regulating NMPs and their descendants in post-gastrulation mouse embryos. *Sall4* deletion using *TCre* caused body/tail truncation, reminiscent of early depletion of NMPs, suggesting a role of *Sall4* in NMP maintenance. This phenotype became significant at the time of the trunk-to-tail transition, suggesting that *Sall4* maintenance of NMPs enables tail formation. *Sall4* mutants exhibit expanded neural and reduced mesodermal tissues, indicating a role of *Sall4* in NMP differentiation balance. Mechanistically, we show that *Sall4* promotion of WNT/β-catenin signaling contributes to NMP maintenance and differentiation balance. RNA-Seq and SALL4 ChIP-Seq analyses support the notion that *Sall4* regulates both mesodermal and neural development. Furthermore, in the mesodermal compartment, genes regulating presomitic mesoderm differentiation are downregulated in *Sall4* mutants. In the neural compartment, we show that differentiation of NMPs towards post-mitotic neuron is accelerated in *Sall4* mutants. Our results collectively provide evidence supporting the role of *Sall4* in regulating NMPs and their descendants.

KEY WORDS: Neuromesodermal progenitors, Body/tail elongation, Sall4, WNT/β-catenin signaling, Mesodermal progenitors and neural progenitors

INTRODUCTION

The vertebrate embryo develops by progressively adding new tissues at the posterior end of the body after gastrulation. Research in the past decade identified the neuromesodermal progenitors (NMPs), which continue to contribute to both neural tube and somites in post-gastrulation vertebrate embryos (Gouti et al., 2015; Henrique et al., 2015; Kimelman, 2016; Steventon and Martinez Arias, 2017). This finding challenged the conventional view of segregation of three germ layers during gastrulation and impacted on the developmental biology field. NMPs are characterized by the co-expression of the transcription factors SOX2 and T (brachyury, T-box transcription factor T). High levels of expression of *Sox2* and *T* are required for development of the neural lineage and the mesodermal lineage, respectively (Martin and Kimelman, 2012; Olivera-Martinez et al., 2012; Tsakiridis et al., 2014). NMPs express low levels of T and SOX2 and are detected in the node-streak boarder and the caudal lateral epiblast during body elongation (Garriock et al., 2015; Wymeersch et al., 2016). NMPs are later relocated in the chordoneural hinge of the tail bud, where the posterior neural plate overlies the caudal notochord, and continue to contribute to the elongating tail (Aires et al., 2018). In addition, the expression of *Nkx1.2* also marks NMPs and other progenitors (Rodrigo Albors et al., 2018). Recent comparison of NMPs in different model systems suggested that NMPs in mouse embryos expand during trunk development and decrease in the tail bud until the embryo terminates tail elongation (Berenguer et al., 2018; Steventon and Martinez Arias, 2017; Wymeersch et al., 2016). Therefore, it is considered that maintenance of NMPs and continued production of neural and paraxial mesoderm (PM) progenitors significantly contribute to the development of the spinal cord and PM-derived tissues in the trunk and tail.

Mouse mutant analyses have provided insights into the maintenance and fate choice of NMPs. Genetic studies show that WNT/β-catenin signaling and T maintain NMPs; embryos with mutations in WNT/β-catenin signaling components or *T* exhibit severe body truncation due to early depletion of NMPs (Beddington et al., 1992; Cunningham et al., 2015; Galceran et al., 1999; Martin and Kimelman, 2010; Takada et al., 1994). In addition, fibroblast growth factor (FGF) signaling and Cdx genes interact with WNT/β-catenin signaling for NMP maintenance and body elongation (Amin et al., 2016; Diez Del Corral and Morales, 2017). During the fate choice between neural and PM progenitors, defects in the WNT/β-catenin–T regulatory loop cause expansion of neural tissues and reduction of PM, suggesting that WNT/β-catenin signaling promotes NMP differentiation toward the mesodermal lineage (Garriock et al., 2015; Martin and Kimelman, 2012). The WNT/β-catenin–T loop regulates another T-box gene, *Tbx6*, which functions in early fate choice of NMPs into mesoderm (Javali et al., 2017; Koch et al., 2017; Nowotschin et al., 2012; Takemoto et al., 2011). In contrast, retinoic acid plays a role in promoting differentiation into neural fate (Cunningham et al., 2016; Gouti et al., 2017). Although these reports provide molecular clues to the regulation of NMPs, the molecular mechanisms for NMP maintenance and differentiation are still under active investigation.

[1]Department of Genetics, Cell Biology and Development, University of Minnesota, 321 Church St. SE, Minneapolis, MN 55455, USA. [2]Stem Cell Institute, University of Minnesota, 2001 6th St. SE, Minneapolis, MN 55455, USA. [3]Developmental Biology Center, University of Minnesota, 321 Church St. SE, Minneapolis, MN 55455, USA. [4]Lillehei Heart Institute, University of Minnesota, 2231 6th St. SE, Minneapolis, MN 55455, USA. [5]Department of Kidney Development, Institute of Molecular Embryology and Genetics, Kumamoto University, Kumamoto, Japan 860-0811. [6]Department of Neuroscience, University of Minnesota, 321 Church St. SE, Minneapolis, MN 55455, USA. [7]Paul and Sheila Wellstone Muscular Dystrophy Center, University of Minnesota, 516 Delaware St. SE, Minneapolis, MN 55455, USA.
*Present address: Department of Biochemistry and Molecular Biology, Mayo Clinic, Rochester, MN 55905, USA.

‡Author for correspondence (kawak005@umn.edu)

W.G., 0000-0002-3147-4028; Y.K., 0000-0002-0043-9705

Received 5 March 2019; Accepted 18 June 2019

Development (2019) 146, dev177659. doi:10.1242/dev.177659

After NMPs make the neural versus PM fate decision, those descendants transition to more differentiated cell types within neural and mesodermal compartments, respectively. During neural fate transition, NMPs reach pre-neural tube (PNT) status and express *Nkx1.2* and *Sox2*, and then differentiate into neural progenitors (Gouti et al., 2015; Rodrigo Albors et al., 2018). These cells start to express a specific combination of transcription factors that define distinct progenitor domains in response to patterning signals. For instance, ventral neural progenitors start to express OLIG2, followed by activation of NKX2.2 and subsequently FOXA2 in a more ventral domain, in a mutually exclusive manner. The expression of OLIG2, NKX2.2 and FOXA2 in the ventral neural tube defines progenitor domains for pMN, p3 and floor plate, respectively (Dessaud et al., 2008; Le Dréau and Martí, 2012). The pMN and p3 progenitors further differentiate into the post-mitotic motor neurons and V3 interneurons, respectively. During mesodermal fate transition, NMPs migrate into the presomitic mesoderm (PSM), which involves *msgn1* and *tbx16* (paralog of mouse *Tbx6*) in zebrafish (Bouldin et al., 2015; Manning and Kimelman, 2015). In the PSM, *Tbx6* and *Msgn1* promote PM progenitor differentiation (Chalamalasetty et al., 2014; Javali et al., 2017). As PM cells migrate anteriorly, they become more differentiated under the control of WNT, FGF and NOTCH signaling, in which *Hes7* orchestrates oscillatory gene expression patterns to periodically form paired somites (Hubaud and Pourquié, 2014).

Sall4 is a member of the Sall gene family, which encodes zinc finger transcription factors (de Celis and Barrio, 2009; Sweetman and Münsterberg, 2006). *Sall4* is highly expressed in pluripotent embryonic stem cells (ESCs) and preimplantation mouse embryos (Elling et al., 2006; Miller et al., 2016; Sakaki-Yumoto et al., 2006). In ESCs, recent studies suggest that *Sall4* is a key regulator of the pluripotency transcriptional network and cell cycle progression (Miller et al., 2016; Yuri et al., 2009). In preimplantation mouse embryos, *Sall4* is involved in the lineage commitment of inner cell mass cells of the blastocyst to the epiblast and primitive endoderm (Miller et al., 2017 preprint). In post-implantation stages, *Sall4* is highly expressed in the epiblast, and *Sall4* null embryos die shortly after implantation prior to gastrulation (Elling et al., 2006; Sakaki-Yumoto et al., 2006). In the late gastrulation and post-gastrulation stages, *Sall4* is strongly expressed in the caudal part of the body, including the area in which NMPs are detected (Kohlhase et al., 2002; Tahara et al., 2018b). The early lethality of *Sall4*$^{-/-}$ embryos hampered the investigation of *Sall4* functions in post-implantation embryos. We previously reported that *Sall4* conditional knockout (cKO) using *TCre* caused defects in hindlimb development (Akiyama et al., 2015). In this study, we found that *TCre; Sall4* cKO neonates exhibit tail truncation, a phenotype observed in mutants with early depletion of NMPs (Beddington et al., 1992; Galceran et al., 1999; Garriock et al., 2015; Herrmann, 1992; Takada et al., 1994). We show that *Sall4* is necessary for maintenance of NMPs and neural versus mesodermal differentiation balance of NMPs in post-gastrulation mouse embryos. We further provide genetic evidence that *Sall4* plays a role in NMP descendants by regulating differentiation in both mesodermal and neural compartments.

RESULTS

Conditional deletion of *Sall4* causes depletion of NMPs and tail truncation

During the analysis of *TCre; Sall4* cKO mutants (Akiyama et al., 2015), we found that mutant neonates exhibited tail truncation and disorganized vertebrae, specifically from the posterior thoracic (20th) to the lumbar (26th) vertebrae (Fig. 1A-B″). This suggests

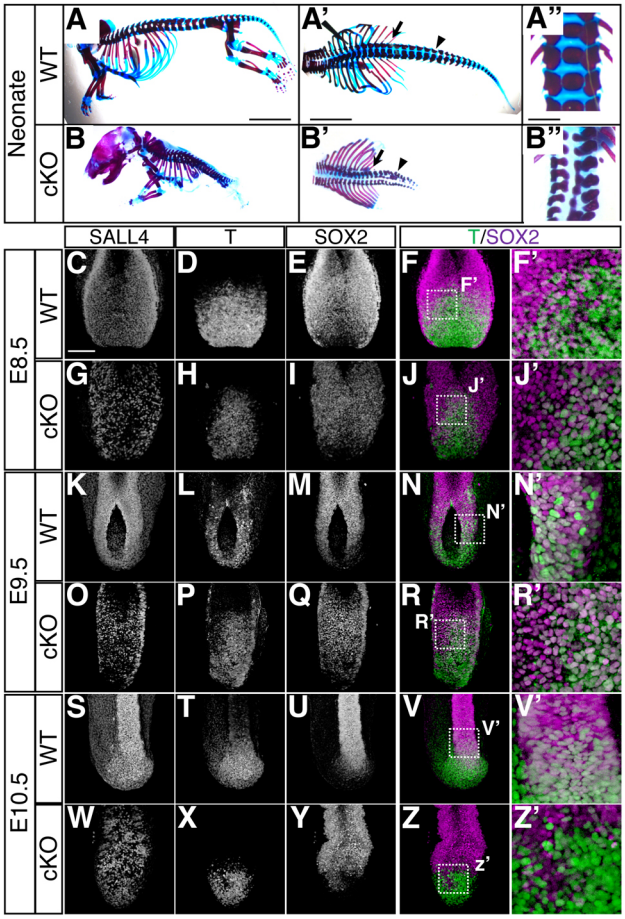

Fig. 1. *Sall4* deletion leads to early NMP depletion and body truncation. (A-B″) Lateral (A,B) and dorsal (A′,B′) views of WT and *Sall4* cKO neonatal mice stained with Alcian Blue and Alizarin Red. Arrows and arrowheads in A′ and B′ point to the most posterior thoracic and lumber vertebrae, respectively. In the upper-left corner of A′ the edge of the forceps can be seen. A″ and B″ show dorsal views of vertebrae at the thoracic to lumber level. (C-Z′) Whole-mount immunofluorescence images of the caudal part of the body of WT and *Sall4* cKO embryos at E8.5 (C-J′), E9.5 (K-R′) and E10.5 (S-Z′). Immunoreactivities for the indicated antibodies are shown. F′,J′,N′,R′,V′,Z′ are magnifications of the boxed areas in F,J,N,R,V,Z, which are shown as overlays of T (green) and SOX2 (magenta) signals. Scale bars: 5 mm (A-B′); 1 mm (A″,B″);100 µm (C-Z).

developmental defects become significant at E9.0-9.75 (20-28 somite stages). Although we previously confirmed efficient deletion of *Sall4* by E8.5 through *Sall4* mRNA *in situ* hybridization (Akiyama et al., 2015), it is possible that the SALL4 protein persists after the mRNA becomes undetectable. Therefore, we examined SALL4 immunoreactivity in the posterior part of the body in whole-mount embryos and sections. We also simultaneously detected T and SOX2 in order to evaluate how SALL4 deletion impacts NMPs.

We found that SALL4 immunoreactivity was reduced, but still detectable in a speckled manner at E8.5 in whole-mount *Sall4* mutants, compared with wild-type (WT) controls (n=10; Fig. 1C,G). By section immunofluorescence, SALL4 signals in the mesenchyme were significantly reduced in mutant embryos. SALL4 signals in the epithelial primitive streak, where NMPs are located (Garriock et al., 2015), were detectable, although downregulation was evident (n=3; Fig. S1A). At this stage, approximately 50% of cells in the posterior part of *Sall4* mutants lost SALL4 immunoreactivity (Fig. S1B), but WT and *Sall4* mutant

Development (2019) 146, dev177659. doi:10.1242/dev.177659

embryos are morphologically indistinguishable. $T^+/SOX2^+$ cells were detected in the caudal lateral epiblast of *Sall4* mutants (Fig. 1D-F′,H-J′, Fig. S1A). Quantitative analysis indicated that the ratio of $T^+/SOX2^+$ cells was lower in *Sall4* mutants than WT (Fig. S1C, Table S1), indicating a reduced NMP population before morphological alterations at E8.5. At E9.5 (20-24 somite stage), SALL4 signals were significantly reduced in the posterior body of *Sall4* cKO embryos in whole-mount analysis (n=6; Fig. 1K,O). Section analysis also showed significant reduction of the SALL4 signals in both the posterior neural plate and mesenchymal tissues (n=3; Fig. S1D). *Sall4* cKO embryos exhibited a delay of neural tube closure and an enlarged posterior neural plate. $T^+/SOX2^+$ cells were reduced in number but still detected in the more medial region compared with WT embryos, possibly owing to the delayed neural tube closure (Fig. 1L-N′,P-R′, Fig. S1D, Table S1). At E10.5, SALL4 signals were undetectable in the mesoderm and were weakly detectable in a speckled manner in the neural tube by whole-mount staining (n=6; Fig. 1S,W). Section analysis confirmed a significant reduction of SALL4 in both neural and mesenchymal tissues (n=3; Fig. S1E). $T^+/SOX2^+$ cells were not detected in the tail bud of *Sall4* mutants at E10.5, whereas double-positive cells were detected in WT embryos (Fig. 1T-V′,X-Z′, Fig. S1E,F, Table S1). The early depletion of $T^+/SOX2^+$ cells in *Sall4* mutants compared with WT embryos supports the notion that *Sall4* is necessary for NMP maintenance.

These results show a correlation between reduction of SALL4 immunoreactivity and depletion of $T^+/SOX2^+$ cells, which further correlates with tail truncation and disorganized vertebrae in *Sall4* mutants. These results collectively suggest that *Sall4* plays a role in NMP maintenance and body/tail elongation.

Sall4 deletion causes an imbalance between neural versus mesodermal tissues

The enlarged posterior neural plate in *Sall4* cKO embryos suggests defects in the balance of differentiation. To assess this possibility, we simultaneously detected $SOX2^+$ neural and $LEF1^+$ mesodermal tissues in the posterior end of the embryo. We used LEF1 instead of T, because T expression is downregulated when mesodermal progenitors further differentiate. We found that the width of the $SOX2^+$ posterior neural plate is enlarged in *Sall4* mutants, compared with WT (Fig. 2A,B). Moreover, $LEF1^+$ mesoderm tissue seems to be thinner in *Sall4* mutants at E9.5. The reduction of the mesoderm tissue, visualized by T plus LEF1, became more evident in *Sall4* mutants at E10.5 (Fig. 2C). Although the increased neural tube width at E9.5 may involve a mechanical failure relating to delayed neural tube closure, these results demonstrate that loss of *Sall4* led to increased neural tissue and reduced mesoderm development.

We further evaluated neural and mesodermal tissues in more detail by section immunofluorescence at the level of the PSM. Because of the delayed neural tube closure in *Sall4* mutants at E9.5, we sectioned E10.5 embryos at the middle of the PSM. The ratio of $LEF1^+$ mesoderm cells over total $DAPI^+$ cells was reduced in *Sall4* mutants, compared with WT (Fig. 2D,H,L). In contrast, the ratio of $SOX2^+$ neural cells was elevated (Fig. 2E,I,L). Similarly, percentage of $LEF1^+$ mesoderm out of the total area was reduced, and the $SOX2^+$ neural area was elevated (Fig. 2M). We also detected a significant reduction of cell proliferation and increased apoptosis in both mesodermal and neural tissues in *Sall4* mutants (Fig. 2F,G,J, K,N,O). Therefore, reduced mesodermal cells and increased neural cells are unlikely to be caused by cell type-specific proliferation and/or cell death. Although the *T* lineage includes other progenitor

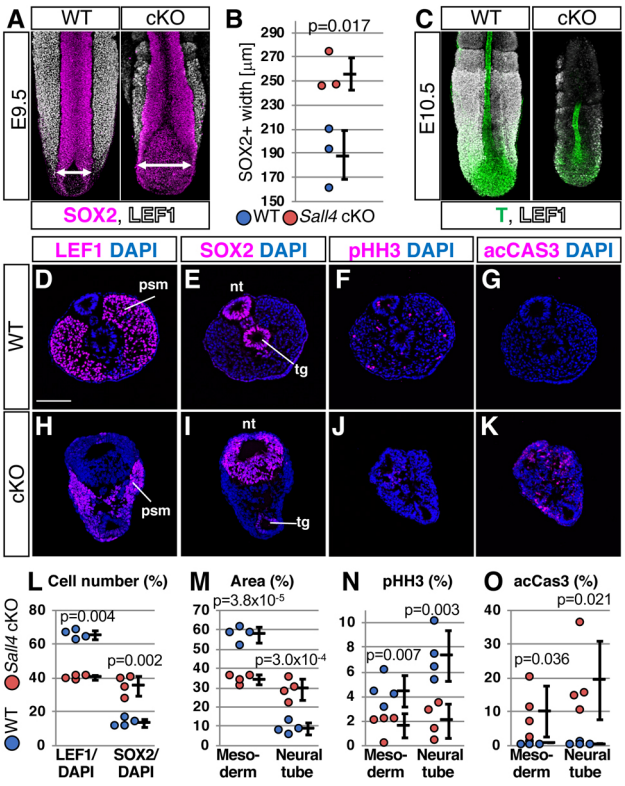

Fig. 2. *Sall4* deletion causes increased neural tissue and decreased mesodermal tissue. (A) Whole-mount WT and *Sall4* cKO embryos at E9.5 stained with antibodies for SOX2 (magenta) and LEF1 (white). (B) Graph of the width of the widest region of the posterior neural plate/tube at E9.5 (shown by double-headed arrows in A, n=3). Shown are mean±s.d. The P-value by unpaired t-test is shown. (C) Whole-mount WT and *Sall4* cKO embryos at E10.5 stained with antibodies for T (green) and LEF1 (white). (D-K) Immunofluorescence of LEF1, SOX2, phosphohistone H3 (pHH3) and activated caspase 3 (acCAS3) in the PSM levels of WT (D-G) and *Sall4* cKO (H-K) embryos at E10.5. (L) Quantification of $LEF1^+$ nuclei and $SOX2^+$ nuclei in the neural tube without tail gut per total nuclei of the section. (M) Quantification of $LEF1^+$ mesoderm area and $SOX2^+$ neural tube area per all $DAPI^+$ area of the section. (N) Quantification of $pHH3^+$ cells in the mesoderm area and in the neural tube area per total nuclei of the section. (O) Quantification of $acCAS3^+$ cells in the mesoderm area and in the neural tube area per total nuclei of the section. Shown are mean±s.d. P-values are shown in each panel (unpaired t-test). n=4 for both WT and *Sall4* cKO. nt, neural tube; psm, presomitic mesoderm; tg, tail gut. Scale bar: 100 µm.

populations, these results support the notion that the balance between neural versus PM fate choice from NMPs was disrupted in *Sall4* mutants.

Sall4 mutants exhibit increased neural and reduced mesodermal molecular programs

Next, we performed transcriptome analysis to characterize molecular changes in *Sall4* mutants. We dissected the tissue posterior to the 20th somite levels, where SALL4 was significantly reduced at E9.5, and performed RNA-Seq. The transcriptome showed broad changes of expression of neural and mesodermal genes in *Sall4* mutants (Fig. 3A, Figs S2 and S3). With a P-value cutoff of 0.05 and absolute fold change greater than 1.5, we found 98 and 13 dysregulated neuron differentiation (GO:0030182) and mesoderm development (GO:0007498) related genes, respectively. Although *Sall4* mutants exhibited reduced mesoderm and expanded neural tube, these genes with neural or mesodermal GO terms

Development (2019) 146, dev177659. doi:10.1242/dev.177659

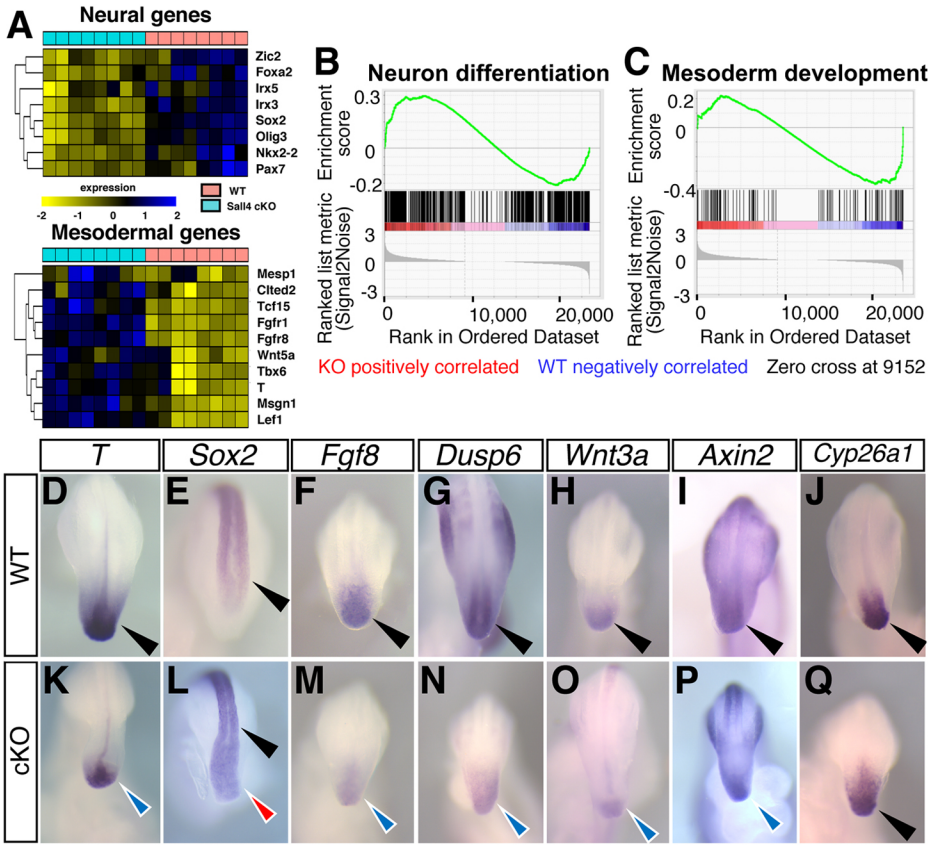

Fig. 3. *Sall4* deletion causes changes of expression of genes related to NMP maintenance and neural and mesodermal genes. (A) Heat map of genes with GO term as neural genes (upper) and mesoderm genes (lower) in WT versus *Sall4* cKO. (B,C) GSEA analysis of genes with GO terms of neural differentiation (B) and mesoderm development (C) among genes that are differentially expressed in WT versus *Sall4* cKO posterior tissue. (D-Q) Whole-mount *in situ* hybridization of the indicated genes in WT (D-J) and *Sall4* cKO (K-Q) at E9.5. Black arrowheads point to normal expression in the posterior tip of the body in WT embryos and *Sox2* and *Cyp26a1* expression in the *Sall4* cKO embryo. Blue arrowheads point to reduced expression in *Sall4* cKO embryos (K,M-P). Red arrowhead in L points to upregulated *Sox2* expression in the *Sall4* cKO embryo.

included both upregulated and downregulated genes (Figs S2 and S3). Because of the altered neural versus mesodermal balance in *Sall4* cKO embryos, we tested the hypothesis that the dysregulated genes in *Sall4* mutants are significantly associated with the mesoderm and neural differentiation/development functions. We performed Gene Set Enrichment Analysis (GSEA) (Subramanian et al., 2005) using 107 known genes related to mesoderm development (GO:0007498). We also performed GSEA using 500 known genes randomly chosen from the 1378 neuron differentiation genes (GO:0030182). The reported GSEA *P*-values for neuron differentiation and mesoderm development were both <0.001 (Fig. 3B,C), which indicated that the mesoderm development and neuron differentiation functions are significantly enriched in the differentially expressed genes. We additionally performed Fisher's exact test by using all the 1378 genes with the neuron GO term, which also showed a significant increase in the number of differentially expressed neural genes in *Sall4* mutants (P=2.945e-07). These results are consistent with the immunofluorescence data and support the notion that mesodermal and neural differentiation are impaired in *Sall4* mutants.

Correlating with the tail truncation in *Sall4* mutant neonates, genes that are known to regulate NMPs and body elongation are consistently downregulated in the transcriptome (Fig. 3A). Consistent with our immunofluorescence analysis (Fig. 1, Fig. S1), we detected reduced expression of *T* and higher expression of *Sox2* by whole-mount *in situ* hybridization (Fig. 3D,E,K,L). Strong *Sox2* expression extended further into the posterior edge of the neural plate in *Sall4* cKO embryos, compared with WT. Expression of *Fgf8* and *Wnt3a*, necessary for NMP maintenance and body elongation (Henrique et al., 2015), were downregulated (Fig. 3F,H,M,O). Expression of *Dusp6* and *Axin2*, targets of FGF signaling and WNT signaling, respectively, were also downregulated (Fig. 3G,I,N,P). In contrast, the expression pattern of *Cyp26a1*, which is required to degrade retinoic acid in the posterior part of the body (Abu-Abed et al., 2001; Sakai et al., 2001), did not exhibit significant reduction (Fig. 3J,Q). At E10.5, the reduction of expression of these genes, including *Cyp26a1*, became more significant (Fig. S4). These changes of expression pattern support the idea that loss of *Sall4* causes defects in the WNT-T-FGF regulatory system, which subsequently causes downregulation of *Cyp26a1*.

Given the known roles of WNT/β-catenin signaling in NMPs (Gouti et al., 2015; Henrique et al., 2015; Kimelman, 2016), we further characterized activation of WNT/β-catenin signaling in more detail by immunofluorescence. We simultaneously stained whole-mount E9.5 embryos with antibodies against T, SOX2 and active β-catenin (Fig. 4A-D). The fluorescent images show that *Sall4* mutants exhibited reduced levels of nuclear β-catenin, compared with WT. Furthermore, analysis of β-catenin signal intensity in each cell also supported the notion that nuclear β-catenin levels are reduced in *Sall4* mutants (Fig. S5). By using nuclear DAPI signals in every layer of images, we confirmed the presence or absence of T, SOX2 and nuclear active β-catenin signals, and constructed a map of cell distribution of each marker combination (Fig. 4B,D,E). The map showed an increased distribution of cells without nuclear active β-catenin, indicating reduced WNT/β-catenin signaling in *Sall4* mutants. Within each of the three populations of T- and/or SOX2-positive cells, the ratio of nuclear active β-catenin^{+} cells was reduced in *Sall4* mutants (Table 1). These analyses support the idea that reduction of WNT/β-catenin signaling is a mechanism for the defects in NMPs in *Sall4* mutants.

Development (2019) 146, dev177659. doi:10.1242/dev.177659

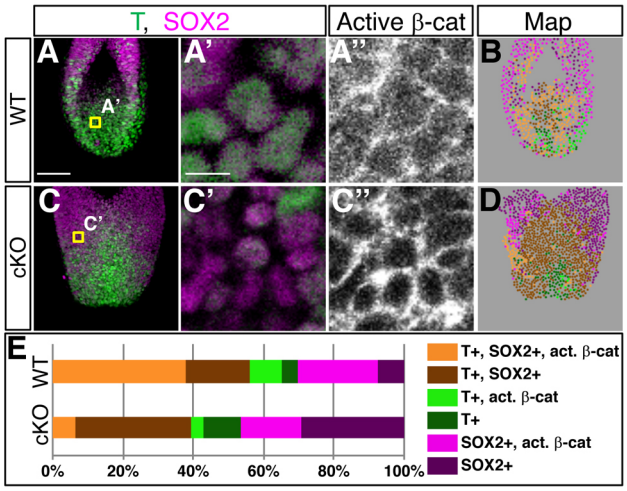

Fig. 4. Downregulation of WNT/β-catenin signaling in *Sall4* cKO embryos. (A,C) Stacked confocal images of whole-mount-stained WT and *Sall4* cKO embryos at E9.5. (A′,A″,C′,C″) Single-layer images of embryos stained for T (green), SOX2 (magenta) and active β-catenin. Shown are high magnifications of single-layer images in the areas indicated in A or C. (B,D) Stacked maps of cells with different combinations of T, SOX2 and active β-catenin with the color code shown in E. (E) Quantification of cells with different combinations of T, SOX2 and active β-catenin (as shown in B and D). *n*=4 for WT, *n*=3 for *Sall4* cKO. Scale bars: 100 µm (A,C); 10 µm (A′,A″,C′,C″).

SALL4-binding sites are enriched in neural and mesodermal genes

In order to further gain insights into *Sall4* functions, we performed SALL4 ChIP-Seq experiments. Because vertebrate defects in *Sall4* cKO neonates are likely derived from defects in PM, we collected tissues posterior to the PSM/somite boundary at E9.5 (Fig. 5A). This tissue included the caudal progenitor zone and PSM but excluded the neural tissue (hereafter referred to as the posterior tissue). We first compared SALL4-enriched sequences in the posterior tissues and in ESCs (Miller et al., 2016). Among 35,756 sequences bound by SALL4 in the posterior tissues, only 4.2% was also bound by SALL4 in ESCs, indicating significantly different binding sites in two cell/tissue types (Fig. 5B). Next, we analyzed locations of SALL4-bound sequences, in which we defined promoter regions as sequences within 10 kb upstream from the transcription start site. Although SALL4 binding to intergenic sequences (46.6%) and introns (26.8%) is significant in the posterior tissues, enrichment in these sites was less frequent than in ESCs (53.5% and 40.2% of bound sequences in intergenic and introns, respectively). Instead, SALL4 binding to the promoters, 5′UTRs and exons was noticeably higher in the posterior tissue than SALL4 binding to such sites in ESCs. The Binomial test suggested that the proportion of SALL4 ChIP-Seq peaks located in transcription start site/promoter/5′UTR regions in the posterior tissues was significantly higher than in ESCs (20.4% versus 3.49%, P<2.2e-16) (Fig. 5C). The distribution of peaks that are bound by SALL4 in both the posterior tissue and mESCs was more similar to the peak distribution in posterior tissue than to that in mESCs. The top-enriched motifs of SALL4-bound sequences in the posterior tissue included motifs for ETS, androgen receptor, YY2 zinc finger factor and ZBTB3 (Fig. S6). These motifs are in contrast to top-enriched motifs in mESCs, such as motifs of OCT4 (POU5F1), ESRRB, KLF and SOX (Fig. S6) (Miller et al., 2016). The difference of motifs indicates that *Sall4* function is cell/tissue-context dependent.

A significant fraction of SALL4-bound sequences in the posterior tissue can be directly assigned to specific genes based on binding to promoters (17.1%), 5′UTRs (3.3%), exons (7.2%) or introns (26.8%). We tested whether SALL4 binding is enriched in genes with mesodermal or neural GO terms by GSEA. Out of 109 genes with mesodermal GO, 95 genes are enriched by SALL4. For genes with neural GO, out of the 500 randomly selected genes,

Table 1. Statistical examination of nuclear β-catenin accumulation in cell populations between WT and *Sall4* cKO posterior tissue

Tested hypothesis	*P*-value
$T^+/SOX2^+$/nuc β-cat$^+$ ratio in $T^+/SOX2^+$ is different between WT and *Sall4* cKO	<2.2e-16
$T^+/SOX2^-$/nuc β-cat$^+$ ratio in $T^+/SOX2^-$ is different between WT and *Sall4* cKO	<2.2e-16
$T^-/SOX2^+$/nuc β-cat$^+$ ratio in $T^-/SOX2^+$ is different between WT and *Sall4* cKO	<2.2e-16

Two-proportion *Z*-test was used to examine differences.
nuc β-cat, nuclear β-catenin.

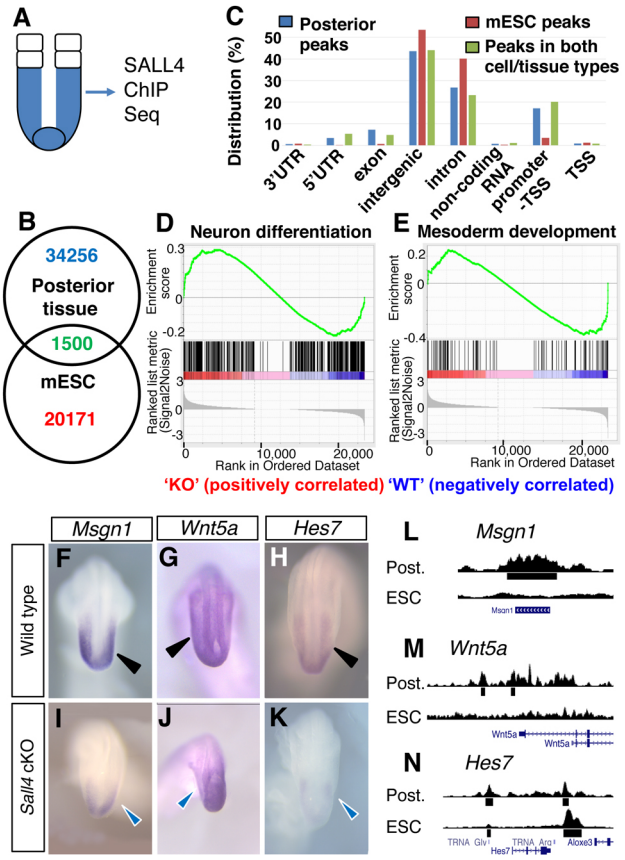

Fig. 5. SALL4 ChIP-Seq analysis of the posterior tissue and downregulation of mesoderm differentiation genes in *Sall4* cKO embryos. (A) Schematic of dissected posterior tissue (blue) for SALL4 ChIP-Seq analysis. (B) Venn diagram for SALL4-enriched sequence numbers in the posterior tissue and mESCs. (C) Distributions of SALL4-enriched sequences in the posterior tissue, mESCs and both cell/tissue types. (D,E) GSEA analysis of genes with GO terms of neural differentiation (D) and mesoderm development (E) among genes that are enriched by SALL4 in the posterior tissue. (F-K) Whole-mount *in situ* hybridization of the indicated mesodermal genes in WT and *Sall4* cKO embryos at E9.5. Black arrowheads point to normal expression in WT PSM (F-H). Blue arrowheads point to reduced expression in the PSM in *Sall4* cKO embryos (I-K). (L-N) Visual representation of SALL4 ChIP-Seq results of the indicated gene loci. Post., the posterior tissue.

Development (2019) 146, dev177659. doi:10.1242/dev.177659

367 genes were enriched by SALL4. The GSEA indicated that genes with mesoderm development and neuron differentiation functions are significantly enriched in the genes that have SALL4 ChIP-Seq peaks (Fig. 5D,E). Although the posterior tissue used in the ChIP-Seq experiments is not homogeneous, the caudal progenitor zone is also enriched in the posterior tissue, in addition to the PSM. Accordingly, we found SALL4 enrichment in some genes that are known to regulate NMPs (Table S2). These genes include *Cdx2*, *T* and *Sox2*. In summary, the results of ChIP-Seq and RNA-Seq together support the idea that SALL4 regulates NMPs as well as mesodermal and neural differentiation of NMP descendants.

Sall4 regulates nascent mesoderm differentiation

Posterior axial skeletal defects in *Sall4* cKO neonates suggest that loss of *Sall4* caused mesodermal differentiation defects in PSM. Consistent with this idea, the expression pattern of *Msgn1*, a master regulator of PSM differentiation (Chalamalasetty et al., 2014; Yoon and Wold, 2000), was severely downregulated (Fig. 5F,I). *Wnt5a*, which is required for outgrowth of the tail (Yamaguchi et al., 1999), was downregulated in the PSM, but not in the posterior neural plate (Fig. 5G,J). *Hes7*, which regulates oscillation of gene expression in the PSM (Bessho et al., 2001), was also downregulated (Fig. 5H,K). These genes are bound by SALL4 (Fig. 5L-N), which is consistent with the GSEA data and suggests a direct regulation of these genes by SALL4. These data support the role of *Sall4* in promoting mesodermal differentiation in the PSM.

Loss of *Sall4* causes accelerated neural differentiation

Next, we asked whether loss of *Sall4* by *TCre* also affects differentiation within the neural compartment. The expression of *Nkx1.2*, a marker for NMPs and PNT cells, was detected in the posterior end of the neural plate and its immediate anterior region of the neural tube of WT embryos (Fig. 6A). In *Sall4* mutants, *Nkx1.2* was expressed in the expanded posterior end of the neural plate, but its expression in the posterior neural tube was undetectable (Fig. 6A,E). Similarly, expression of *Sox2*, a marker for NMPs, PNT cells and neural progenitor cells, was extended into the posterior end of the neural plate in *Sall4* mutants (Fig. 3E,L). Given the reduction of T^+/$SOX2^+$ NMP number in *Sall4* mutants, the expression pattern of *Nkx1.2* and *Sox2* implies that more PNT cells are present in the posterior neural plate but they are absent in the posterior neural tube in *Sall4* mutants. Weak expression of *Sox1*, a neural progenitor marker, was detected in the posterior end of the neural plate of *Sall4* mutants at both mRNA and protein levels, which was not detected in WT embryos (Fig. 6B,C,F,G). These results support the idea that differentiation of NMPs to neural progenitors through the PNT status is accelerated in *Sall4* mutants.

We next asked whether differentiation of neural progenitors is also affected in *Sall4* mutants. Neural progenitors in the ventral neural tube express OLIG2, followed by NKX2.2 and then FOXA2, in a progressively ventrally localized manner. The onset of their expression correlates with the progression of neural progenitor differentiation (Dessaud et al., 2008, 2007). We examined the expression pattern of these markers to assess neural differentiation status by using somite number-matched embryos for careful comparison of WT and *Sall4* mutants. Furthermore, we used outgrowth of hindlimb buds and expression of PLZF (ZBTB16) in the hindlimb mesenchyme (Akiyama et al., 2015) in adjacent sections in order to identify sections representing posterior hindlimb levels (Fig. S7). At E9.75 (27/28 somite stage), OLIG2 is expressed in the ventral neural tube, whereas NKX2.2 is undetectable at the

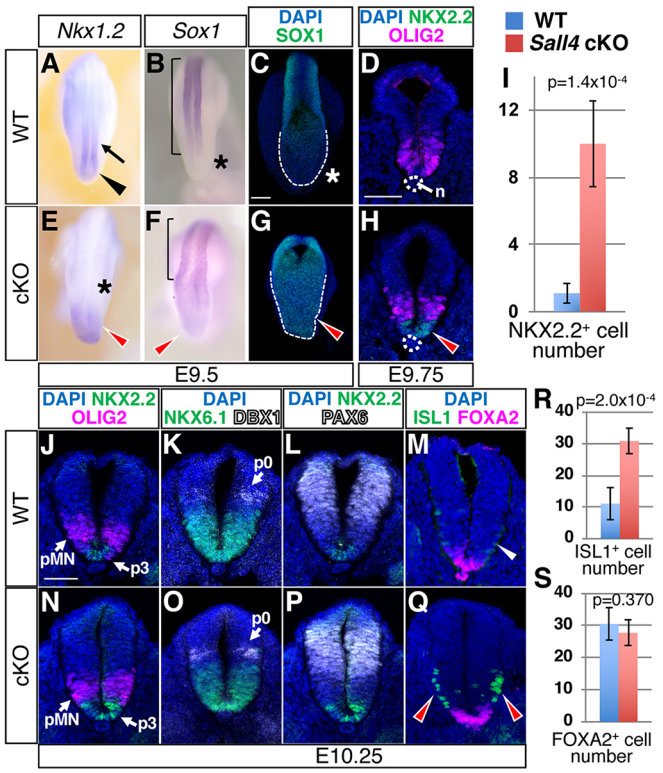

Fig. 6. Accelerated neural patterning and differentiation in the posterior region of *Sall4* cKO embryos. (A,B,E,F) *In situ* hybridization of *Nkx1.2* and *Sox1* at E9.5 in WT (A,B) and *Sall4* cKO (E,F) embryos. Black arrowhead and arrow in A point to expression in the posterior neural plate and the posterior neural tube, respectively. Red arrowheads point to increased (E) or ectopic (F) expression. Asterisks mark lack of expression. Bracket indicates *Sox1* expression in the neural tube. (C,G) Confocal images of SOX1 expression in the posterior of whole-mount embryos. Dashed lines indicate posterior end of the neural plate. Red arrowhead points to ectopic expression of SOX1 (G). Asterisk indicates a lack of SOX1 signals at the posterior end of the neural plate (C). (D,H) Immunofluorescence of OLIG2 (magenta) and NKX2.2 (green) in WT (D) and *Sall4* cKO (H) embryos at E9.75 (27/28 somite stage). Red arrowhead points to $NKX2.2^+$ cells in *Sall4* cKO embryos. Dotted circle indicates the notochord (n). (I) Quantification of $NKX2.2^+$ cells at the posterior hindlimb level at E9.75. Graphs shows numbers of cells (mean±s.d.) per section. *P*-values by unpaired *t*-test are shown. $n=5$ for WT, $n=6$ for *Sall4* cKO. (J-Q) Immunofluorescence of the indicated markers in WT (J-M) and *Sall4* cKO (N-Q) embryos at E10.25 (33/34 somite stage). White and red arrowheads point to $ISL1^+$ cells at the posterior hindlimb level in WT (M) and *Sall4* cKO (Q) embryos, respectively. In K and O, DBX1 signals are shown in white. (R,S) Quantification of $ISL1^+$ cells (R) and FOXA2+ cells (S) at the posterior hindlimb level at E10.25. Graphs show numbers of cells (mean±s.d.) per section. *P*-values by unpaired *t*-test are shown within each panel. $n=5$ for both WT and *Sall4* cKO. Scale bars: 100 µm (C,G); 50 µm (D,H,J-Q).

posterior hindlimb level in WT (Fig. 6D). In contrast, NKX2.2 is expressed in the ventral-most neural tube between the two dorsally positioned OLIG2 domains (Fig. 6H,I), indicating precocious neural differentiation in *Sall4* mutants. At E10.25 (33/34 somite stage), the p3, pMN and p0 domains express NKX2.2, OLIG2 and DBX1, respectively, in a ventral-to-dorsal order in both WT and *Sall4* mutants (Fig. 6J,K,N,O). NKX6.1, which marks ventral progenitors, and PAX6, which marks an intermediate region, did not show changes of their domain (Fig. 6K,L,O,P, Fig. S8). These expression patterns suggest that the gross patterning of neural tube along the dorsoventral axis is not altered in *Sall4* mutants. At the same stage, we found that *Sall4* mutants exhibited a significantly greater number of ISL1-expressing cells at the hindlimb level,

Development (2019) 146, dev177659. doi:10.1242/dev.177659

compared with WT embryos (Fig. 6M,Q,R). As *Isl1* is an essential gene for post-mitotic motor neuron identity (Dessaud et al., 2008), this result indicates precocious appearance of motor neurons in *Sall4* mutants. These results suggest that the progression of neural patterning and differentiation is accelerated in *Sall4* mutants. Examination of FOXA2-expressing floor plate cell numbers showed no significant differences between WT and *Sall4* cKO embryos at the hindlimb level (Fig. 6M,Q,S), suggesting that the increased number of ISL1-expressing cells is unlikely to be caused by increased floor plate cells, which produce the ventral morphogen sonic hedgehog. Unlike the hindlimb, numbers of ISL-expressing cells at the forelimb level were slightly lower in *Sall4* mutants than in WT embryos (Fig. S9), at which level *Sall4* mutants do not exhibit significant defects (Fig. 1A,B). These results support the idea that differentiation of NMP descendants in the neural compartment is promoted in *Sall4* mutants.

DISCUSSION

We propose a model whereby *Sall4* plays multiple roles in the posterior part of the embryo (Fig. 7). *Sall4* participates in the maintenance of and neural versus mesodermal differentiation balance of NMPs. *Sall4* might also be involved in the transition of NMPs from the trunk to the tail bud during body elongation. In addition, *Sall4* promotes mesodermal differentiation and restricts neural differentiation of NMP descendants. Involvement of *Sall4* in the regulation of multiple processes in developing embryos complicates the analyses of *Sall4* function. Several studies have developed protocols for an *in vitro* derivation of NMP-like cells and their differentiation from pluripotent stem cells (Gouti et al., 2014; Lippmann et al., 2015; Tsakiridis et al., 2014; Turner et al., 2014). Such an *in vitro* approach will help further dissect roles of *Sall4* in multiple steps of regulation of NMPs and their descendants *in vitro*.

Mouse mutants with defects in WNT/β-catenin signaling show severe body truncation posterior to the forelimb bud level due to early depletion of NMPs (Galceran et al., 1999; Takada et al., 1994). The axial levels of defects in these mutants are consistent with the observation that NMPs contribute to tissues posterior to the 6th somite level (forelimbs develop at 7-12 somite levels) (Henrique et al., 2015; Tzouanacou et al., 2009). In contrast, *TCre; Sall4* mutants exhibited truncation at the tail level. This difference would involve SALL4 protein that has been produced before *TCre*-mediated disruption of the *Sall4* gene, compared with null alleles used in other studies. *Sall4* is highly expressed in the epiblast at early post-implantation stages before *TCre*-mediated recombination (Sakaki-Yumoto et al., 2006). The pre-existing SALL4 protein might be stable and persist after *Sall4* gene abrogation, which is consistent with our immunofluorescence analysis of *Sall4* cKO embryos. The timing of significant SALL4 depletion in *Sall4* mutants allowed us to investigate *Sall4* function separated from gastrulation. Therefore, even though the truncation defects of *Sall4* mutants are milder than those observed in other mutants, our data support the role of *Sall4* in NMP maintenance and body/tail elongation *in vivo*.

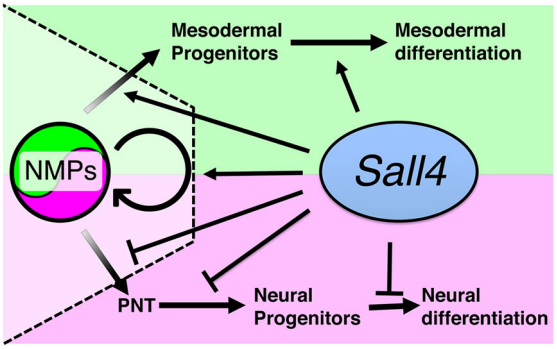

Fig. 7. A model of *Sall4* function in NMPs and their descendants in the mouse embryo. Proposed functions of *Sall4* for NMP maintenance and regulation of differentiation between mesodermal versus neural fate, promotion of mesodermal differentiation and restriction of neural differentiation of NMP descendants. For more detail see Discussion.

The tail truncation of *Sall4* mutants also suggests a possibility that *Sall4* regulates transition of NMPs from the trunk to the tail. A lineage-tracing experiment indicated that NMPs are a continuous cell population that contributes to the trunk and tail (Tzouanacou et al., 2009). Recent studies indicated that *Gdf11*-dependent transition of NMPs from the trunk into the tail bud is required for tail elongation (Jurberg et al., 2013). This transition occurs around E9.5, which correlates with the timing at which *Sall4* cKO embryos exhibit defects in the posterior of the body (Aires et al., 2018). Tail elongation involves distinct mechanisms from the trunk, such as the *Gdf11-Lin28-Hox13* system (Aires et al., 2019; Aires et al., 2016; Robinton et al., 2019). Therefore, it is also possible that *Sall4* regulates the NMP transition into the tail bud and tail-specific elongation mechanisms. This possibility does not rule out the possibility that *Sall4* directly regulates NMPs. Further analysis with cell type-specific and fine-temporal dissection of function of *Sall4* would enhance our understanding of NMP biology and trunk-tail elongation.

Our study suggests that *Sall4* promotion of WNT/β-catenin signaling is a mechanism for *Sall4* regulation of NMPs. Previous studies showed that SALL4 can interact with β-catenin when transfected *in vitro* and can enhance WNT/β-catenin signaling in luciferase reporter assays (Hobbs et al., 2012). In addition, *Sall4* and *Ctnnb1* genetically interact to regulate anterior-posterior axis formation in mouse embryos (Uez et al., 2008). Consistent with these reports, we observed reduction of WNT/β-catenin signaling in the posterior part of *Sall4* cKO embryos. It has been shown that WNT/β-catenin signaling is essential for NMP maintenance (Gouti et al., 2015; Henrique et al., 2015; Kimelman, 2016), and NMP differentiation into mesodermal lineages (Garriock et al., 2015; Martin and Kimelman, 2012), and acts upstream of *Tbx6* to regulate PSM differentiation (Dunty et al., 2008). Therefore, *Sall4* promotion of WNT/β-catenin signaling could act as a mechanism for these functions. The *TCre; Sall4* mutants exhibited an expanded neural tube, but not the formation of a supernumerary neural tube observed in *Wnt3a*$^{-/-}$ mutants (Garriock et al., 2015). Owing to the use of the conditional inactivation strategy and SALL4 stability discussed above, SALL4 protein depletes gradually in *TCre; Sall4* mutants from E8.5 to E10.5. Residual SALL4 may be responsible for gradual downregulation of β-catenin signaling rather than abolishment, which could have caused the difference of an ectopic neural tube formation. It should be noted that the precise mechanisms by which *Sall4* regulates WNT/β-catenin signaling in the posterior body remain to be determined. The SALL4 enrichment near *Cdx2*, *T* and *Sox2* observed in our ChIP-Seq experiment also suggests that *Sall4* may directly regulate these genes for NMP maintenance. In addition, *Sall4* may genetically interact with Cdx genes to regulate NMPs, as a *sall4-cdx4* interaction is reported to regulate hematopoiesis in the lateral plate mesoderm in zebrafish (Paik et al., 2013). Further study will help fully understand how *Sall4* regulates NMPs and their descendants. In the case of mesodermal differentiation, our ChIP-Seq data suggest that

Development (2019) 146, dev177659. doi:10.1242/dev.177659

SALL4 also directly regulates some genes in the PM, including *Msgn1*. A previous study demonstrated that *Msgn1* is a target of WNT/β-catenin signaling (Chalamalasetty et al., 2011), and *Sall4* might also promote *Msgn1* expression through WNT/β-catenin signaling. Thus, the defects in the mesodermal tissue in *Sall4* mutants could be mediated, in part, by reduced *Msgn1* expression. However, $Msgn1^{-/-}$ embryos exhibit an expanded *T* expression domain, opposite to what we observed in *Sall4* mutants (Chalamalasetty et al., 2014; Yoon and Wold, 2000). This difference suggests that *Msgn1* also functions in parallel with *Sall4*, as a master regulator of PM development.

In mESCs, SALL4 inhibits neural differentiation (Miller et al., 2016). In the posterior tissue, *Sall4* also restricts neural differentiation, which is observed as precocious neural patterning and differentiation in *Sall4* mutants. However, SALL4-bound sequences are significantly different in ESCs and the posterior tissue, suggesting that mechanisms of *Sall4* regulation of neural differentiation are different in ESCs and the posterior tissue. One explanation for this difference is the possibility that SALL4 acts with other cell type-specific transcription factors. In this scenario, SALL4 regulates different downstream genes depending on its partners. Another possible mechanism is direct regulation of neural differentiation genes by SALL4 in the posterior tissues, which is supported by significant enrichment of SALL4 targets in the neural differentiation GO.

It has been noted that some cell types in the trunk, such as spinal cells and skeletal muscle, are difficult to generate from pluripotent stem cells *in vitro* (Gouti et al., 2014). Recent progress in the derivation and directed differentiation of NMPs from pluripotent stem cells strongly suggested that anterior neural plate and posterior trunk neurons have distinct developmental origins (Henrique et al., 2015). According to this idea, NMPs contribute to trunk neurons, such as spinal motor neurons, during body/tail elongation. Generation and characterization of trunk neural cell types through NMPs is a topic of wide interest with the potential for therapeutic application (Gouti et al., 2015; Verrier et al., 2018). Recent reports demonstrated that manipulation of retinoic acid, hedgehog and BMP/TGFβ signaling can alter neural differentiation from NMPs (Cunningham et al., 2016; Gouti et al., 2014; Lippmann et al., 2015; Verrier et al., 2018). Therefore, accelerated neural patterning and differentiation in the absence of *Sall4* in NMPs and their descendants offer a possibility of manipulating neural differentiation *in vitro* through regulating functions of *Sall4* in combination with these signaling pathways.

MATERIALS AND METHODS

Animal breeding, skeletal preparation and *in situ* hybridization

Embryos were collected by timed mating of $Sall4^{fl/fl}$ females and $TCre^{Tg/Tg}$; $Sall4^{+/fl}$ males (Akiyama et al., 2015). Alcian Blue/Alizarin Red skeletal staining and whole-mount *in situ* hybridization were performed as previously described (Akiyama et al., 2015). Three to five embryos per probe per stage were examined by whole-mount *in situ* hybridization. Animal breeding was performed according to approval of the Institutional Animal Care and Use Committee of the University of Minnesota.

Immunofluorescence

For whole-mount staining, embryos were fixed in 4% paraformaldehyde (PFA) at 4°C for 2 h, then washed with PBS+0.1% Triton X-100 (PBSTr), blocked with 5% donkey serum in PBSTr for 60 min at room temperature, and stained and rocked overnight with primary antibodies at 4°C. After washing with PBSTr, embryos were stained with secondary antibodies at 4°C overnight, washed, and incubated with DAPI solution. For section staining, cryosections of 14 µm thickness were treated as previously described (Akiyama et al., 2015; Tahara et al., 2018a). Antibodies and working dilutions are listed in Table S3. Images were acquired using a Zeiss LSM710 confocal microscope with Zen software.

Quantification of neural versus mesodermal differentiation

For analysis of neural versus mesodermal tissues (shown in Fig. 2), E10.5 embryos were cryosectioned at the PSM level and stained with anti-SOX2 and anti-LEF1. We acquired three section images at the middle of the PSM from each embryo, and the average cell count or area measurement was used as representative data of each embryo. The total number of cells, $LEF1^+$ cells, $SOX2^+$ cells, $pHis3^+$ cells and activated caspase 3^+ cells were counted using ImageJ. WT (n=4) and *Sall4* cKO (n=4) embryos were analyzed, and significance was determined by unpaired *t*-test.

Quantification of T, SOX2 and active β-catenin signals from whole-mount samples

After whole-mount staining, embryos were mounted on glass-bottom dishes using low melting agarose. Fluorescent images were acquired every 1 µm along the *z*-axis until we obtained the widest part of the embryos (15-20 images/embryo). We evaluated whether each of $DAPI^+$ nucleus possessed overlapping signals of T, SOX2 and/or active β-catenin using Photoshop, and constructed a map of each layer. The final map was generated by overlaying all maps.

Quantification of markers in the neural tube

Using PLZF signals and hindlimb bud morphologies of adjacent sections, we chose two sections from each embryo, which represented the levels of the posterior part of the hindlimbs. Cells with $FOXA2^+$, $ISL1^+$, $NKX2.2^+$ or $OLIG2^+$ signals were counted using ImageJ. The average cell count of two sections was used as representative data of each embryo. Five embryos (both WT and *Sall4* cKO) were analyzed for each graph, and significance was determined by unpaired *t*-test.

RNA-Seq and ChIP-Seq

Tissues posterior to somite level 20 were collected from E9.5 embryos and total RNA was purified using the RNeasy micro kit (Qiagen). Strand-specific RNA-Seq libraries were created using the Illumina Library Creation System with 0.5 µg of RNA. Sequencing (50 base paired end, v4 chemistry, 20 million reads per sample) was performed with HiSeq2500 at the University of Minnesota Genomic Center. Data were analyzed by TopHat and Bowtie (Trapnell et al., 2012).

For ChIP-Seq, tissues posterior to the boundary of the PSM and the somite were collected from E9.5 WT embryos. Tissues were kept in PBS on ice during dissection, and treated with dispase (1.5 mg/ml, Roche, 4942078001, 37°C, 5 min), followed by removal of the neural tube in cold PBS. The remaining tissue (the posterior tissue) was dissociated using TrypLE (Invitrogen) at 37°C for 5 min, neutralized with DMEM+10% fetal bovine serum, and collected by low speed centrifugation. Approximately 100 embryos were used per sample. Cells were treated following a previously published procedure (Kanda et al., 2014; Park et al., 2012). Cells were fixed with 1% PFA in Crosslinking buffer (100 mM NaCl, 1 mM EDTA, 0.5 mM EGTA, 50 mM HEPES) for 5 min at room temperature. The reaction was stopped by adding 1/10 volume of 1.25 M glycine on ice for 5 min. Cells were collected by low speed centrifugation, and stored at −80° C until a sufficient amount of cells (1.0×10^7 per sample) were collected. Cells were subjected to sonication using the truChip Chromatin Shearing Reagent kit (Covaris, PN 520154) with a Covaris S220 (peak power: 105 W; duty factor: 2%; cycles/burst: 200; water temperature: 4°C; total processing time: 5 min). Dynabeads (50 µl, Thermo Fisher, 10003D) were coupled with the 10 µg of anti-SALL4 antibody (Abcam, ab29112) for 30 min at room temperature, and incubated with sheared chromatin overnight at 4°C. The Dynabeads were washed with washing buffer (50 mM HEPES, pH7.5, 0.5 M LiCl, 1% NP-40, 1% sodium deoxycholate, 1 mM EDTA) six times. The immunoprecipitated complexes were eluted and reverse-crosslinked from the beads by adding elution buffer (50 mM Tris-HCl, pH 8, 1% SDS, 10 mM EDTA) and heating at 65°C overnight. Immunoprecipitated DNA was treated with RNase A and proteinase K, and

purified for library synthesis. The sequencing was performed using HiSeq2500 (50 base paired end, 20 million reads per sample). The sequencing data were analyzed with MACS2 (Zhang et al., 2008).

Acknowledgements
We are grateful to Jennifer Kim and Samantha Young for their excellent technical assistance. We are also grateful to Drs Juan Carlos Izpisúa Belmonte, David Lohnes, Michael O'Connor, Virginia Papaioannou and Terry Yamaguchi for sharing materials and/or equipment.

Competing interests
The authors declare no competing or financial interests.

Author contributions
Conceptualization: Y.K.; Formal analysis: N.T., K.C., W.G., P.S., Y.N., Y.K.; Investigation: N.T., H.K., K.Q.C., A.A., M.Y.P., W.G., P.S., S.H., Y.K.; Resources: R.N., Y.N., D.J.G., Y.K.; Writing - original draft: K.Q.C., Y.K.; Writing - review & editing: N.T., H.K., K.Q.C., A.A., M.Y.P., W.G., P.S., S.H., R.N., Y.N., D.J.G., Y.K.; Visualization: Y.K.; Supervision: Y.N., D.J.G., Y.K.; Project administration: Y.K.; Funding acquisition: Y.K.

Funding
This study was supported by grants from the National Institutes of Health (R01AR064195 to Y.K.; R01HL122576 to D.J.G.). Deposited in PMC for release after 12 months.

Data availability
RNA-Seq and ChIP-Seq data have been deposited in the Sequence Read Archive database under BioProject accession number PRJNA525663.

Supplementary information
Supplementary information available online at
http://dev.biologists.org/lookup/doi/10.1242/dev.177659.supplemental

References
Abu-Abed, S., Dolle, P., Metzger, D., Beckett, B., Chambon, P. and Petkovich, M. (2001). The retinoic acid-metabolizing enzyme, CYP26A1, is essential for normal hindbrain patterning, vertebral identity, and development of posterior structures. *Genes Dev.* **15**, 226-240. doi:10.1101/gad.855001

Aires, R., Jurberg, A. D., Leal, F., Nóvoa, A., Cohn, M. J. and Mallo, M. (2016). Oct4 is a key regulator of vertebrate trunk length diversity. *Dev. Cell* **38**, 262-274. doi:10.1016/j.devcel.2016.06.021

Aires, R., Dias, A. and Mallo, M. (2018). Deconstructing the molecular mechanisms shaping the vertebrate body plan. *Curr. Opin. Cell Biol.* **55**, 81-86. doi:10.1016/j.ceb.2018.05.009

Aires, R., de Lemos, L., Nóvoa, A., Jurberg, A. D., Mascrez, B., Duboule, D. and Mallo, M. (2019). Tail bud progenitor activity relies on a network comprising Gdf11, Lin28, and Hox13 genes. *Dev. Cell* **48**, 383-395.e388. doi:10.1016/j.devcel.2018.12.004

Akiyama, R., Kawakami, H., Wong, J., Oishi, I., Nishinakamura, R. and Kawakami, Y. (2015). Sall4-Gli3 system in early limb progenitors is essential for the development of limb skeletal elements. *Proc. Natl. Acad. Sci. USA* **112**, 5075-5080. doi:10.1073/pnas.1421949112

Amin, S., Neijts, R., Simmini, S., van Rooijen, C., Tan, S. C., Kester, L., van Oudenaarden, A., Creyghton, M. P. and Deschamps, J. (2016). Cdx and T Brachyury co-activate growth signaling in the embryonic axial progenitor Niche. *Cell Rep.* **17**, 3165-3177. doi:10.1016/j.celrep.2016.11.069

Beddington, R. S., Rashbass, P. and Wilson, V. (1992). Brachyury–a gene affecting mouse gastrulation and early organogenesis. *Development*, **Suppl.**, 157-165.

Berenguer, M., Lancman, J. J., Cunningham, T. J., Dong, P. D. S. and Duester, G. (2018). Mouse but not zebrafish requires retinoic acid for control of neuromesodermal progenitors and body axis extension. *Dev. Biol.* **441**, 127-131. doi:10.1016/j.ydbio.2018.06.019

Bessho, Y., Sakata, R., Komatsu, S., Shiota, K., Yamada, S. and Kageyama, R. (2001). Dynamic expression and essential functions of Hes7 in somite segmentation. *Genes Dev.* **15**, 2642-2647. doi:10.1101/gad.930601

Bouldin, C. M., Manning, A. J., Peng, Y.-H., Farr, G. H., III, Hung, K. L., Dong, A. and Kimelman, D. (2015). Wnt signaling and tbx16 form a bistable switch to commit bipotential progenitors to mesoderm. *Development* **142**, 2499-2507. doi:10.1242/dev.124024

Chalamalasetty, R. B., Dunty, W. C., Jr., Biris, K. K., Ajima, R., Iacovino, M., Beisaw, A., Feigenbaum, L., Chapman, D. L., Yoon, J. K., Kyba, M. et al. (2011). The Wnt3a/beta-catenin target gene Mesogenin1 controls the segmentation clock by activating a Notch signalling program. *Nat. Commun.* **2**, 390. doi:10.1038/ncomms1381

Chalamalasetty, R. B., Garriock, R. J., Dunty, W. C., Jr., Kennedy, M. W., Jailwala, P., Si, H. and Yamaguchi, T. P. (2014). Mesogenin 1 is a master regulator of paraxial presomitic mesoderm differentiation. *Development* **141**, 4285-4297. doi:10.1242/dev.110908

Cunningham, T. J., Kumar, S., Yamaguchi, T. P. and Duester, G. (2015). Wnt8a and Wnt3a cooperate in the axial stem cell niche to promote mammalian body axis extension. *Dev. Dyn.* **244**, 797-807. doi:10.1002/dvdy.24275

Cunningham, T. J., Colas, A. and Duester, G. (2016). Early molecular events during retinoic acid induced differentiation of neuromesodermal progenitors. *Biol. Open* **5**, 1821-1833. doi:10.1242/bio.020891

de Celis, J. F. and Barrio, R. (2009). Regulation and function of Spalt proteins during animal development. *Int. J. Dev. Biol.* **53**, 1385-1398. doi:10.1387/ijdb.072408jd

Dessaud, E., Yang, L. L., Hill, K., Cox, B., Ulloa, F., Ribeiro, A., Mynett, A., Novitch, B. G. and Briscoe, J. (2007). Interpretation of the sonic hedgehog morphogen gradient by a temporal adaptation mechanism. *Nature* **450**, 717-720. doi:10.1038/nature06347

Dessaud, E., McMahon, A. P. and Briscoe, J. (2008). Pattern formation in the vertebrate neural tube: a sonic hedgehog morphogen-regulated transcriptional network. *Development* **135**, 2489-2503. doi:10.1242/dev.009324

Diez Del Corral, R. and Morales, A. V. (2017). The multiple roles of FGF signaling in the developing spinal cord. *Front. Cell Dev. Biol.* **5**, 58. doi:10.3389/fcell.2017.00058

Dunty, W. C., Jr., Biris, K. K., Chalamalasetty, R. B., Taketo, M. M., Lewandoski, M. and Yamaguchi, T. P. (2008). Wnt3a/beta-catenin signaling controls posterior body development by coordinating mesoderm formation and segmentation. *Development* **135**, 85-94. doi:10.1242/dev.009266

Elling, U., Klasen, C., Eisenberger, T., Anlag, K. and Treier, M. (2006). Murine inner cell mass-derived lineages depend on Sall4 function. *Proc. Natl. Acad. Sci. USA* **103**, 16319-16324. doi:10.1073/pnas.0607884103

Galceran, J., Farinas, I., Depew, M. J., Clevers, H. and Grosschedl, R. (1999). Wnt3a−/−like phenotype and limb deficiency in Lef1(−/−)Tcf1(−/−) mice. *Genes Dev.* **13**, 709-717. doi:10.1101/gad.13.6.709

Garriock, R. J., Chalamalasetty, R. B., Kennedy, M. W., Canizales, L. C., Lewandoski, M. and Yamaguchi, T. P. (2015). Lineage tracing of neuromesodermal progenitors reveals novel Wnt-dependent roles in trunk progenitor cell maintenance and differentiation. *Development* **142**, 1628-1638. doi:10.1242/dev.111922

Gouti, M., Tsakiridis, A., Wymeersch, F. J., Huang, Y., Kleinjung, J., Wilson, V. and Briscoe, J. (2014). In vitro generation of neuromesodermal progenitors reveals distinct roles for wnt signalling in the specification of spinal cord and paraxial mesoderm identity. *PLoS Biol.* **12**, e1001937. doi:10.1371/journal.pbio.1001937

Gouti, M., Metzis, V. and Briscoe, J. (2015). The route to spinal cord cell types: a tale of signals and switches. *Trends Genet.* **31**, 282-289. doi:10.1016/j.tig.2015.03.001

Gouti, M., Delile, J., Stamataki, D., Wymeersch, F. J., Huang, Y., Kleinjung, J., Wilson, V. and Briscoe, J. (2017). A gene regulatory network balances neural and mesoderm specification during vertebrate trunk development. *Dev. Cell* **41**, 243-261.e247. doi:10.1016/j.devcel.2017.04.002

Henrique, D., Abranches, E., Verrier, L. and Storey, K. G. (2015). Neuromesodermal progenitors and the making of the spinal cord. *Development* **142**, 2864-2875. doi:10.1242/dev.119768

Herrmann, B. G. (1992). Action of the Brachyury gene in mouse embryogenesis. *Ciba Foundation Symp.* **165**, 78-86; discussion 86-91. doi:10.1002/9780470514221.ch5

Hobbs, R. M., Fagoonee, S., Papa, A., Webster, K., Altruda, F., Nishinakamura, R., Chai, L. and Pandolfi, P. P. (2012). Functional antagonism between Sall4 and Plzf defines germline progenitors. *Cell Stem Cell* **10**, 284-298. doi:10.1016/j.stem.2012.02.004

Hubaud, A. and Pourquié, O. (2014). Signalling dynamics in vertebrate segmentation. *Nat. Rev.* **15**, 709-721. doi:10.1038/nrm3891

Javali, A., Misra, A., Leonavicius, K., Acharyya, D., Vyas, B. and Sambasivan, R. (2017). Co-expression of Tbx6 and Sox2 identifies a novel transient neuromesoderm progenitor cell state. *Development* **144**, 4522-4529. doi:10.1242/dev.153262

Jurberg, A. D., Aires, R., Varela-Lasheras, I., Nóvoa, A. and Mallo, M. (2013). Switching axial progenitors from producing trunk to tail tissues in vertebrate embryos. *Dev. Cell* **25**, 451-462. doi:10.1016/j.devcel.2013.05.009

Kanda, S., Tanigawa, S., Ohmori, T., Taguchi, A., Kudo, K., Suzuki, Y., Sato, Y., Hino, S., Sander, M., Perantoni, A. O. et al. (2014). Sall1 maintains nephron progenitors and nascent nephrons by acting as both an activator and a repressor. *J. Am. Soc. Nephrol.* **25**, 2584-2595. doi:10.1681/ASN.2013080896

Kimelman, D. (2016). Tales of tails (and Trunks): forming the posterior body in vertebrate embryos. *Curr. Top. Dev. Biol.* **116**, 517-536. doi:10.1016/bs.ctdb.2015.12.008

Koch, F., Scholze, M., Wittler, L., Schifferl, D., Sudheer, S., Grote, P., Timmermann, B., Macura, K. and Herrmann, B. G. (2017). Antagonistic activities of Sox2 and brachyury control the fate choice of neuro-mesodermal progenitors. *Dev. Cell* **42**, 514-526.e517. doi:10.1016/j.devcel.2017.07.021

Kohlhase, J., Heinrich, M., Schubert, L., Liebers, M., Kispert, A., Laccone, F., Turnpenny, P., Winter, R. M. and Reardon, W. (2002). Okihiro syndrome is

caused by SALL4 mutations. *Hum. Mol. Genet.* **11**, 2979-2987. doi:10.1093/hmg/11.23.2979

Le Dréau, G. and Martí, E. (2012). Dorsal-ventral patterning of the neural tube: a tale of three signals. *Dev. Neurobiol.* **72**, 1471-1481. doi:10.1002/dneu.22015

Lippmann, E. S., Williams, C. E., Ruhl, D. A., Estevez-Silva, M. C., Chapman, E. R., Coon, J. J. and Ashton, R. S. (2015). Deterministic HOX patterning in human pluripotent stem cell-derived neuroectoderm. *Stem Cell Rep.* **4**, 632-644. doi:10.1016/j.stemcr.2015.02.018

Manning, A. J. and Kimelman, D. (2015). Tbx16 and Msgn1 are required to establish directional cell migration of zebrafish mesodermal progenitors. *Dev. Biol.* **406**, 172-185. doi:10.1016/j.ydbio.2015.09.001

Martin, B. L. and Kimelman, D. (2010). Brachyury establishes the embryonic mesodermal progenitor niche. *Genes Dev.* **24**, 2778-2783. doi:10.1101/gad.1962910

Martin, B. L. and Kimelman, D. (2012). Canonical Wnt signaling dynamically controls multiple stem cell fate decisions during vertebrate body formation. *Dev. Cell* **22**, 223-232. doi:10.1016/j.devcel.2011.11.001

Miller, A., Ralser, M., Kloet, S. L., Loos, R., Nishinakamura, R., Bertone, P., Vermeulen, M. and Hendrich, B. (2016). Sall4 controls differentiation of pluripotent cells independently of the Nucleosome Remodelling and Deacetylation (NuRD) complex. *Development* **143**, 3074-3084. doi:10.1242/dev.139113

Miller, A., Gharbi, S., Etienne-Dumeau, C., Nishinakamura, R. and Hendrich, B. (2017). Transcriptional control by Sall4 in blastocysts facilitates lineage commitment of inner cell mass cells. *bioRxiv*. doi:10.1101/194852

Nowotschin, S., Ferrer-Vaquer, A., Concepcion, D., Papaioannou, V. E. and Hadjantonakis, A.-K. (2012). Interaction of Wnt3a, Msgn1 and Tbx6 in neural versus paraxial mesoderm lineage commitment and paraxial mesoderm differentiation in the mouse embryo. *Dev. Biol.* **367**, 1-14. doi:10.1016/j.ydbio.2012.04.012

Olivera-Martinez, I., Harada, H., Halley, P. A. and Storey, K. G. (2012). Loss of FGF-dependent mesoderm identity and rise of endogenous retinoid signalling determine cessation of body axis elongation. *PLoS Biol.* **10**, e1001415. doi:10.1371/journal.pbio.1001415

Paik, E. J., Mahony, S., White, R. M., Price, E. N., Dibiase, A., Dorjsuren, B., Mosimann, C., Davidson, A. J., Gifford, D. and Zon, L. I. (2013). A Cdx4-Sall4 regulatory module controls the transition from mesoderm formation to embryonic hematopoiesis. *Stem Cell Rep.* **1**, 425-436. doi:10.1016/j.stemcr.2013.10.001

Park, J.-S., Ma, W., O'Brien, L. L., Chung, E., Guo, J.-J., Cheng, J.-G., Valerius, M. T., McMahon, J. A., Wong, W. H. and McMahon, A. P. (2012). Six2 and Wnt regulate self-renewal and commitment of nephron progenitors through shared gene regulatory networks. *Dev. Cell* **23**, 637-651. doi:10.1016/j.devcel.2012.07.008

Robinton, D. A., Chal, J., Lummertz da Rocha, E., Han, A., Yermalovich, A. V., Oginuma, M., Schlaeger, T. M., Sousa, P., Rodriguez, A., Urbach, A. et al. (2019). The Lin28/let-7 pathway regulates the mammalian caudal body axis elongation program. *Dev. Cell* **48**, 396-405.e393. doi:10.1016/j.devcel.2018.12.016

Rodrigo Albors, A., Halley, P. A. and Storey, K. G. (2018). Lineage tracing of axial progenitors using Nkx1-2CreER(T2) mice defines their trunk and tail contributions. *Development* **145**, dev164319. doi:10.1242/dev.164319

Sakai, Y., Meno, C., Fujii, H., Nishino, J., Shiratori, H., Saijoh, Y., Rossant, J. and Hamada, H. (2001). The retinoic acid-inactivating enzyme CYP26 is essential for establishing an uneven distribution of retinoic acid along the anterio-posterior axis within the mouse embryo. *Genes Dev.* **15**, 213-225. doi:10.1101/gad.851501

Sakaki-Yumoto, M., Kobayashi, C., Sato, A., Fujimura, S., Matsumoto, Y., Takasato, M., Kodama, T., Aburatani, H., Asashima, M., Yoshida, N. et al. (2006). The murine homolog of SALL4, a causative gene in Okihiro syndrome, is essential for embryonic stem cell proliferation, and cooperates with Sall1 in anorectal, heart, brain and kidney development. *Development* **133**, 3005-3013. doi:10.1242/dev.02457

Steventon, B. and Martinez Arias, A. (2017). Evo-engineering and the cellular and molecular origins of the vertebrate spinal cord. *Dev. Biol.* **432**, 3-13. doi:10.1016/j.ydbio.2017.01.021

Subramanian, A., Tamayo, P., Mootha, V. K., Mukherjee, S., Ebert, B. L., Gillette, M. A., Paulovich, A., Pomeroy, S. L., Golub, T. R., Lander, E. S. et al. (2005). Gene set enrichment analysis: a knowledge-based approach for interpreting genome-wide expression profiles. *Proc. Natl. Acad. Sci. USA* **102**, 15545-15550. doi:10.1073/pnas.0506580102

Sweetman, D. and Münsterberg, A. (2006). The vertebrate spalt genes in development and disease. *Dev. Biol.* **293**, 285-293. doi:10.1016/j.ydbio.2006.02.009

Tahara, N., Akiyama, R., Theisen, J. W. M., Kawakami, H., Wong, J., Garry, D. J. and Kawakami, Y. (2018a). Gata6 restricts Isl1 to the posterior of nascent hindlimb buds through Isl1 cis-regulatory modules. *Dev. Biol.* **434**, 74-83. doi:10.1016/j.ydbio.2017.11.013

Tahara, N., Kawakami, H., Zhang, T., Zarkower, D. and Kawakami, Y. (2018b). Temporal changes of Sall4 lineage contribution in developing embryos and the contribution of Sall4-lineages to postnatal germ cells in mice. *Sci. Rep.* **8**, 16410. doi:10.1038/s41598-018-34745-5

Takada, S., Stark, K. L., Shea, M. J., Vassileva, G., McMahon, J. A. and McMahon, A. P. (1994). Wnt-3a regulates somite and tailbud formation in the mouse embryo. *Genes Dev.* **8**, 174-189. doi:10.1101/gad.8.2.174

Takemoto, T., Uchikawa, M., Yoshida, M., Bell, D. M., Lovell-Badge, R., Papaioannou, V. E. and Kondoh, H. (2011). Tbx6-dependent Sox2 regulation determines neural or mesodermal fate in axial stem cells. *Nature* **470**, 394-398. doi:10.1038/nature09729

Trapnell, C., Roberts, A., Goff, L., Pertea, G., Kim, D., Kelley, D. R., Pimentel, H., Salzberg, S. L., Rinn, J. L. and Pachter, L. (2012). Differential gene and transcript expression analysis of RNA-seq experiments with TopHat and Cufflinks. *Nat. Protoc.* **7**, 562-578. doi:10.1038/nprot.2012.016

Tsakiridis, A., Huang, Y., Blin, G., Skylaki, S., Wymeersch, F., Osorno, R., Economou, C., Karagianni, E., Zhao, S., Lowell, S. et al. (2014). Distinct Wnt-driven primitive streak-like populations reflect in vivo lineage precursors. *Development* **141**, 1209-1221. doi:10.1242/dev.101014

Turner, D. A., Hayward, P. C., Baillie-Johnson, P., Rue, P., Broome, R., Faunes, F. and Martinez Arias, A. (2014). Wnt/beta-catenin and FGF signalling direct the specification and maintenance of a neuromesodermal axial progenitor in ensembles of mouse embryonic stem cells. *Development* **141**, 4243-4253. doi:10.1242/dev.112979

Tzouanacou, E., Wegener, A., Wymeersch, F. J., Wilson, V. and Nicolas, J.-F. (2009). Redefining the progression of lineage segregations during mammalian embryogenesis by clonal analysis. *Dev. Cell* **17**, 365-376. doi:10.1016/j.devcel.2009.08.002

Uez, N., Lickert, H., Kohlhase, J., de Angelis, M. H., Kühn, R., Wurst, W. and Floss, T. (2008). Sall4 isoforms act during proximal-distal and anterior-posterior axis formation in the mouse embryo. *Genesis* **46**, 463-477. doi:10.1002/dvg.20421

Verrier, L., Davidson, L., Gierlinski, M., Dady, A. and Storey, K. G. (2018). Neural differentiation, selection and transcriptomic profiling of human neuromesodermal progenitor-like cells in vitro. *Development* **145**, dev166215. doi:10.1242/dev.166215

Wymeersch, F. J., Huang, Y., Blin, G., Cambray, N., Wilkie, R., Wong, F. C. K. and Wilson, V. (2016). Position-dependent plasticity of distinct progenitor types in the primitive streak. *eLife* **5**, e10042. doi:10.7554/eLife.10042

Yamaguchi, T. P., Bradley, A., McMahon, A. P. and Jones, S. (1999). A Wnt5a pathway underlies outgrowth of multiple structures in the vertebrate embryo. *Development* **126**, 1211-1223.

Yoon, J. K. and Wold, B. (2000). The bHLH regulator pMesogenin1 is required for maturation and segmentation of paraxial mesoderm. *Genes Dev.* **14**, 3204-3214. doi:10.1101/gad.850000

Yuri, S., Fujimura, S., Nimura, K., Takeda, N., Toyooka, Y., Fujimura, Y.-I., Aburatani, H., Ura, K., Koseki, H., Niwa, H. et al. (2009). Sall4 is essential for stabilization, but not for pluripotency, of embryonic stem cells by repressing aberrant trophectoderm gene expression. *Stem Cells* **27**, 796-805. doi:10.1002/stem.14

Zhang, Y., Liu, T., Meyer, C. A., Eeckhoute, J., Johnson, D. S., Bernstein, B. E., Nussbaum, C., Myers, R. M., Brown, M., Li, W. et al. (2008). Model-based analysis of ChIP-Seq (MACS). *Genome Biol.* **9**, R137. doi:10.1186/gb-2008-9-9-r137